A model of the muscarinic receptor-induced changes in K^+-current and action potentials in the bullfrog atrial cell

J. M. Shumaker,* J. W. Clark,* W. R. Giles,‡ and G. Szabo§

*Department of Electrical and Computer Engineering, Rice University, Houston, Texas 77251-1892, ‡Departments of Medical Physiology and Medicine, University of Calgary Medical School, Calgary, Alberta, Canada T2N 4N1; and §Department of Physiology and Biophysics, University of Texas Medical Branch, Galveston, Texas 77550

ABSTRACT A model is formulated for characterizing the behavior of the acetylcholine (ACh)-sensitive K^+ membrane channel (muscarinic channel) in bullfrog atrial myocytes. Parameters of the muscarinic current model are chosen in fit available data from the literature on bullfrog atrial myocytes (3, 4, 45). This model is subsequently incorporated into a larger mathematical model of the bullfrog myocyte that is based on quantitative whole-cell voltage clamp data (40). Simulations are conducted on the active atrial cell model in bathing media containing ACh at different concentrations to explore the effect of this muscarinic channel on the electrical behavior of the myocyte. The model predicts a progressive shortening of the action potential with increasing [ACh], as well as an indirect influence of the muscarinic K^+ current on the other membrane currents of the atrial cell. Interpretation of the simulation results provides suggestions for the probable mechanisms underlying the shortening of the action potential due to activity of the muscarinic channel. Specifically, the model predicts that with an increase in ACh concentration: (*a*) the outward muscarinic current, $I_{K,ACh}(t)$, increases in magnitude but shortens in duration; (*b*) the calcium current, $I_{Ca}(t)$, may increase in magnitude, but when it does so it decreases in duration compared with the control conditions; (*c*) the intracellular Ca^{2+} concentration $[Ca^{2+}]_i$ waveform during the action potential decreases in both magnitude and duration.

Because the contractile activity of the cell is controlled by the $[Ca^{2+}]_i$ waveform, the model predicts a decrease in contractile strength with an increase in ACh concentration in the bathing medium; i.e., a negative inotropic effect.

INTRODUCTION

The neurotransmitter acetylcholine (ACh), which is released from parasympathetic nerve endings, has a number of effects at the cellular level that are mediated by muscarinic ACh receptors localized on the sarcolemma. Stimulation of muscarinic receptors is thought to affect at least two membrane currents; it activates an inwardly rectifying potassium current that we shall call the muscarinic channel current $I_{K,ACh}$, and it inhibits the transient inward calcium current I_{Ca}. The slow time course for muscarinic current activation has led to the development of several models that include rate-limiting steps beyond the initial binding of ACh to muscarinic receptors (36, 39). Recent studies of atrial myocytes (3, 4) suggest that opening of a K^+-selective muscarinic channel is mediated by a receptor-activated guanine nucleotide binding G protein (G_K). According to this scheme, opening of these K^+ channels is the result of a cascade of events in which receptor activation by an agonist results first in the activation of G_K, which in turn enhances the probability of this channel opening. G protein activation is accompanied by release of guanosine diphosphate (GDP) and subsequent uptake of guanosine triphosphate (GTP) at a guanine nucleotide binding site (21) located on the α subunit of the G protein which, in its resting form, is a heterotrimer comprised of three subunits termed α, β, and γ (21).

Address correspondence to Dr. J. W. Clark, Jr., Department of Electrical and Computer Engineering, Rice University, P.O. Box 1892, Houston, TX 77251-1892.

G protein activation–deactivation sequence

In the inactive state, G_K consists of a GDP-bound α subunit (α_{GDP}) associated with a $\beta\gamma$ subunit (1, 5, 16, 21). Agonist occupation of the muscarinic receptor results in activation of G_K in which GDP is released from the α subunit resulting in a transient, nucleotide-free state that specifically binds cytoplasmic GTP to form the activated α subunit α_{GTP}. This then leads to dissociation of the heterotrimer into α_{GTP} and $\beta\gamma$ subunits by a process that also requires Mg^{2+} (31). While some uncertainty remains regarding the specific role of G protein subunits in channel activation, there appears to be a general agreement that under physiological circumstances it is the activated α_{GTP} subunit that mediates channel activation (5, 11, 28, 29, 30, 33, 34). The last step in the G protein cycle is the deactivation of the G protein. Eventually, the GTP bound to the α subunit hydrolyzes into α_{GDP} which,

0006-3495/90/03/567/10 $2.00

in the presence of Mg^{2+}, reassociates with the $\beta\gamma$ subunits to form the inactive heterotrimer (1, 5).

The rate limiting step in the activation of the G protein has been discussed in the literature. Breitwieser and Szabo (4) and Ferguson et al. (17) suggest that the rate-limiting step is the dissociation of GDP from the α subunit, whereas Birnbaumer et al. (1) propose that the rate-limiting step occurs during the activation stage after binding of GTP. Breitwieser and Szabo (4) have proposed a simplified two-state kinetic model for the G protein activation–deactivation cycle. These investigators suggest that the rate of GDP release (which they named k_{ACh}) leading to G protein activation is a function of the agonist (ACh) concentration in the extracellular medium, and that the deactivation rate (k_{cat}) is a constant (reference 4, Fig. 13). In this study we employ a reduced two-state model of the activation–deactivation cycle of the G protein that is analogous to the two-state scheme described in Breitwieser and Szabo (4).

Effect of ACh on the slow inward calcium current

The effect of ACh on I_{Ca} in both mammalian and amphibian hearts has also been a topic of considerable interest. In multicellular amphibian and mammalian cardiac tissue preparations, ACh has been shown to reduce I_{Ca} (19, 25, 37, 46). For example, Giles and Noble (19) reported that the primary effect of ACh (at low concentrations) on atrial trabecular strands from bullfrog heart is a reduction in I_{Ca}. Hino and Ochi (25), who performed experiments on guinea pig papillary muscle, found that the slow inward current was decreased in the presence of relatively high ACh concentrations (>0.5 μM). In isolated cardiac myocytes, however, Trautwein and Kameyama (47) report that ACh has a minimal effect on basal I_{Ca}. The effect of ACh on the calcium current is most easily demonstrated in the presence of a β-adrenergic agonist. Specifically, ACh is particularly effective in counteracting the slow inward Ca^{2+} current induced by β adrenergic agonists, which are thought to act by way of a receptor-dependent activation of the G protein G_S. This protein may activate I_{Ca} both directly (48) and indirectly by stimulating membrane-bound adenylate cyclase, thereby elevating the intracellular concentration of cyclic AMP (cAMP) and leading to increased levels of channel phosphorylation by the intermediate of a cAMP-dependent protein kinase (27, 41, 47). Hescheler et al. (24) have concluded that in the presence of a β agonist, ACh reduces I_{Ca} by inhibiting cAMP production, and this reduction is most likely mediated by an inhibitory GTP-binding protein (G_i). Note, however, that in the absence of β-adrenergic stimulation, ACh does not appear to reduce I_{Ca} in rabbit Purkinje fibers (7), frog atrial (22) and ventricular myocytes (18, 22), or guinea pig ventricular myocytes (24). Recent studies confirm that ACh has a relatively small effect on I_{Ca} compared with its effect of ACh on the muscarinic channel in guinea pig atrial myocytes (26), as well as in ferret ventricular myocytes (2). Detailed measurements in both frog atrial and ventricular myocytes (22) and guinea pig atrial myocytes (26) suggest that the reduction of I_{Ca} in the absence of a β agonist is due to a fast activation of the outward current $I_{K,ACh}$, resulting in an "apparent" reduction of the slow inward calcium current, I_{Ca}.

Additional ACh effects

A recent experimental study has also found that ACh can indirectly stimulate the Na^+/K^+ electrogenic pump due to accumulation of extracellular K^+ (23). ACh has also been shown to inhibit the hyperpolarization-activated current (I_f) in rabbit SA node myocytes by way of a negative shift in the I_f activation curve (12, 13, 14) and it has been proposed that this inhibition results from decreased levels of cAMP through a G protein–mediated inhibition of adenylate cyclase activity (15).

MODELING ASPECTS

The present modeling study is focused on the single bullfrog atrial myocyte. This choice provides significant simplifications of this complex problem. First, the hyperpolarization-activated I_f channel present in mammalian pacemaker cells has not been demonstrated in bullfrog myocytes. There have been reports of I_f currents in multicellular voltage clamp studies in bullfrog sinus venosus (9, 10), however, I_f currents have not been observed in whole-cell voltage clamp experiments on individual myocytes (20, 44). In our model we have assumed that the I_f channel is not present. The effect of ACh on the sodium potassium pump is also ignored on the grounds that (*a*) the myocyte being modeled is in a volume conductor of essentially infinite extent and constant ionic composition, which should minimize the effect of ACh (through K^+ accumulation) on the Na^+/K^+ pump; and (*b*) whatever effect ACh has on the Na^+/K^+ pump should be present in the experimental data (reference 4, Fig. 2) and thus would be included in the lumped description of the muscarinic current. The ACh-induced activation of the muscarinic current is also known to exhibit desensitization in high concentrations of ACh (8). However, for the problem at hand, the muscarinic channel model is formulated for relatively low concentrations of ACh for which desensitization is insignificant (4). Therefore, this effect is also ignored in this model.

From the preceding discussions it would appear that in

the absence of a β agonist the major effect of ACh in the frog atrium and ventricle, in ferret ventricle, and guinea pig atrium is to produce an outward current that increases the rate of repolarization (2, 18, 22, 26). In studies on ferret ventricular myocytes (2), the increased rate of repolarization produced by $I_{K,ACh}$ is reported to be responsible for the negative inotropic effect seen in the presence of ACh. Although ACh has been shown to have a significant dose-dependent effect on I_{Ca} in the presence of β agonists (47), this issue will not be addressed in this study. Instead, attention will be focused on the direct effect of ACh on the muscarinic G protein–mediated channel and on the indirect effects that activation of this channel has on the other voltage-dependent channels of the bullfrog atrial myocyte.

A major objective in this study is the development and testing of a simple model of the G protein–activated muscarinic channel in frog atrium. The model is comprised of two states: an activated state and a deactivated state. The process of activation is described by the first order rate coefficient k_*, resulting from a lumped characterization of the intermediate molecular steps occurring between the attachment of ACh to the membrane-bound muscarinic receptor and the subsequent activation of a K^+ channel by G protein. The deactivation process, described by the rate coefficient k_d, is a lumped characterization of the process of GTP hydrolysis that produces the deactivated form of the G protein G_K and ultimately results in the closing of the muscarinic K^+ channel. The mathematical description of this muscarinic channel is discussed below. In whole-cell simulations, the ACh-sensitive K^+ channel is inserted as a parallel branch in the atrial cell model and is allowed to interact with the other inward and outward currents of the model.

The mathematical form chosen for the model of the ACh-sensitive K^+ channel is based partly on an earlier model developed by Osterrieder, Noma, and Trautwein (38) for the muscarinic channel in the rabbit SA node cell. A brief summary of the steps involved in the formulation of the modified description of the muscarinic channel current is as follows. The muscarinic current $I_{K,ACh}$ was chosen to be a product of a voltage- and agonist-dependent gating variable (a) and the ion-transfer characteristic ($\bar{I}_{K,ACh}$) of the channel, that is

$$I_{K,ACh} = a \times \bar{I}_{K,ACh}, \tag{1}$$

where a is the solution of the reaction rate equation

$$\dot{a} = k_*(1 - a) - k_d a \tag{2}$$

and $\bar{I}_{K,ACh}$ is defined as

$$\bar{I}_{K,ACh}(V) = \frac{G\{\exp[0.04(V - E_K)] - 1\}}{\exp\{0.04[V - (E_K + 55)]\}}. \tag{3}$$

In a functional sense the variable a behaves as a Hodgkin–Huxley type gating variable for the channel, with an activation rate constant k_* and deactivation rate constant k_d; G is a gain parameter (.0264) associated with the ion transfer process. Reversal potential measurements of $I_{K,ACh}$ have shown that it is carried by potassium (4, 35, 43, 45). To mathematically model the rate coefficients k_* and k_d, the steady state I–V data from Breitwieser and Szabo (4) was extrapolated to 1 μM ACh, and the dominant slow time constant from the data of Simmons and Hartzell (45) at the same ACh concentration was chosen as the time constant of relaxation for the channel. In accordance with Hodgkin–Huxley theory, τ is defined as

$$\tau = (k_* + k_d)^{-1}. \tag{4}$$

The steady state solution for Eq. 1 is:

$$I_{K,ACh,\infty} = \left(\frac{k_*}{k_d + k_*}\right)\bar{I}_{K,ACh} = k_*\tau\bar{I}_{K,ACh}. \tag{5}$$

Here k_* may be determined by employing the experimental data for both $I_{K,ACh,\infty}$ and τ at an ACh concentration of 1 μM. Thus, knowing k_* and τ, the deactivation rate constant k_d is described using Eq. 4. To match the data from Breitwieser and Szabo (4) in the voltage range more negative to -85 mV, the activation rate constant k_* was chosen to be a function of voltage as well as ACh concentration. The half-activation level for the binding of ACh to the receptor is chosen to be 159 nM in agreement with Breitwieser and Szabo (4). The equations for the rate coefficients of the muscarinic channel model are given below:

$$k_* = \overline{k_*}(1 - 0.69\eta), \tag{6}$$

where

$$\overline{k_*} = \frac{0.00647}{1 + \frac{0.4}{[ACh]}} \tag{7}$$

$$\eta = \frac{1}{1 + \exp\left(\frac{V + 55}{10}\right)} \tag{8}$$

$$k_d = \psi - k'_*, \tag{9}$$

where

$$\psi = \frac{1 + \exp\left(\frac{V + 60}{10}\right)}{260 + 110\exp\left(\frac{V + 60}{10}\right)}. \tag{10}$$

Here k'_* is k_* evaluated at 1 μM ACh.

The behavior of variables associated with the muscarinic channel model are therefore characterized as functions of membrane voltage (V) and ACh concentration according to Eqs. 1–3 and Eqs. 6–10. (In this study the following ACh concentrations were used: 0.03, 0.1, 0.3, 1.0, 3.0, and 6 μM. These concentrations are denoted on some of the waveforms by numbers 1–6). Note that k_* is a function of ACh concentration as well as voltage, however k_d is a function of voltage alone.

COMPUTATIONAL ASPECTS

The complete set of equations describing the atrial cell model is given in Rasmusson et al. (reference 40, Appendix), while the mathematical description of the muscarinic channel is given in Eqs. 1–10 of this paper. The overall differential equation model was implemented on a Sequent Symmetry multiprocessor system comprised of 20 CPUs. Computer code was written in the C programming language and the current, gating variable, and derivative computations were performed in parallel using seven processors. Choosing to solve the system in parallel promoted the direct integration of the gating variables, as opposed to the use of alternative methods such as the Rush–Larsen exponential approximation method (42). A variable step size Sarafyan embedding type of modification to the Runge–Kutta formulas (32) was used for the numerical integration of the model equations. The lower and upper limits on local truncation error were chosen as 10^{-4} and 10^{-6}, respectively. The step size in the algorithm was doubled if the local truncation error was less than the lower limit, and halved if the error was greater than the upper limit.

RESULTS

In this study of the effects of ACh on the membrane currents, the muscarinic channel current model was inserted as an independent parallel branch into an existing atrial myocyte model developed earlier by our group (Rasmusson et al. [40]). Fig. 1 *A* shows model-generated atrial action potentials and Fig. 1 *B* illustrates four of the underlying membrane currents (I_{Ca}, I_K, I_{K1}, $I_{K,ACh}$) in a bathing medium with and without 0.1 μM ACh. The left side of Fig. 1 are the simulated results in the control condition while the right side of Fig. 1 are the results in a 0.1-μM ACh bathing medium. Note that in the presence of ACh, the duration of the action potential shown in Fig. 1 *A* is reduced. Fig. 1 *B* demonstrates the relative magnitudes and time courses of the component membrane ionic currents that generate these action potential waveforms. A 4-ms depolarizing current pulse of 1.2 nA

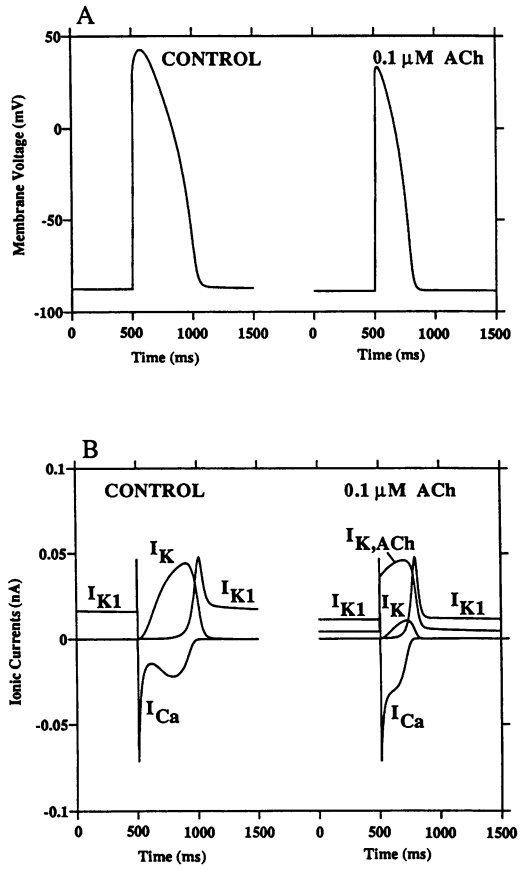

FIGURE 1 Model-generated action potential and transmembrane ionic currents (I_{Ca}, I_K, I_{K1}, and $I_{K,ACh}$) with and without ACh in the bathing medium. The control condition with no ACh in the bath is shown on the left side of these panels, whereas the effects of stimulation with a steady ACh concentration level of 0.1 μM are shown at the right.

was used to elicit the action potentials shown in Fig. 1. In the control condition the sodium current I_{Na} (not shown) is responsible for the initial depolarization of the action potential, a smaller calcium current I_{Ca} then sustains this depolarization forming the plateau, while the delayed rectifier K^+ current I_K is responsible for the onset of repolarization. The inwardly rectifying K^+ current I_{K1} is instrumental in both setting the resting potential of the atrial cell and contributing to the late phase of repolarization. As shown in Fig. 1 *B*, the I_{Ca} waveform consists of an initial inward spike followed by a slower secondary "hump". The latter is attributed to the incomplete inactivation of the calcium channel which is discussed below. The Na^+/K^+ pump and the Na^+/Ca^{2+} exchanger are voltage and ion concentration dependent, however, they contribute only a relatively minor current throughout most of the action potential. The electrogenic calcium pump is dependent on $[Ca^{2+}]_i$ and provides a small outward calcium current.

On the other hand, in the presence of a bath ACh

concentration of 0.1 μM, the characteristics of both the action potential and the underlying membrane currents dramatically change as shown in Fig. 1 *A* and *B*. Note that the ACh-mediated K^+ current ($I_{K,ACh}$) is a very significant current throughout the cardiac cycle. Furthermore, $I_{K,ACh}$ has extremely fast dynamics and thus can mask I_{Ca} during the early phase of the action potential. The simulation shown in Fig. 1 *B* illustrates that the magnitude of the delayed rectifier current I_K can be dramatically reduced in the presence of 0.1 μM ACh. Here $I_{K,ACh}$ is sufficiently large by itself to bring about an early repolarization of the action potential; and I_K has less time to activate in the presence of ACh. The calcium current waveform I_{Ca} is also different than that illustrated in the absence of ACh. In the latter case, the I_{Ca} waveform exhibits a prominent secondary hump. However, in the presence of 0.1 μM ACh, the secondary hump does not develop.

In modeling the electrical behavior of cardiac cells, an important feature of any model is the mechanism utilized for sustaining the "plateau" phase of the action potential. The major inward current sustaining the plateau is the slow inward calcium current I_{Ca}. This current exhibits an initial inward spike followed by a slower "secondary hump" (Fig. 1 *B*). The secondary hump in the waveform is caused by the phenomenon of incomplete inactivation which has been demonstrated experimentally in the work of Campbell et al. (6) and has been mathematically modeled by Rasmusson et al. (40). A thorough understanding of the factors influencing the time course of the I_{Ca} waveform is fundamental to an understanding of the indirect effects of ACh on both normal atrial action potentials, as well as the "slow action potentials" produced by blocking the inward sodium channel via application of tetrodotoxin (TTX) to the bathing medium.

Fig. 2 is included to provide more detailed information on the time course of the I_{Ca} waveform with and without 0.1 μM ACh in the bathing medium. Here, the action potential waveforms are shown in panel *A* (control simulation is labeled *C* and the 0.1 μM ACh simulation is labeled *A*), the activation (*d*) and inactivation (*f*) variables which gate the calcium current are shown in panel *B* (the subscripts *A* and *C* denote the control simulation and the 0.1 μM simulation, respectively), and the resulting I_{Ca} waveform is shown in panel *C* (*C* is the control condition and *A* is the 0.1 μM condition).

In the control simulation, the initial spike portion of I_{Ca} is caused by the fast time course of the activation variable *d*, which increases rapidly from a value of 0 to a value of 1, and is coincident with the leading edge of the action potential. At the beginning of the action potential, the inactivation gating variable *f* has an initial value of 1. Note, however, from Fig. 2 *B*, that *f* declines very slowly compared with the increase in *d*. In addition, the initial

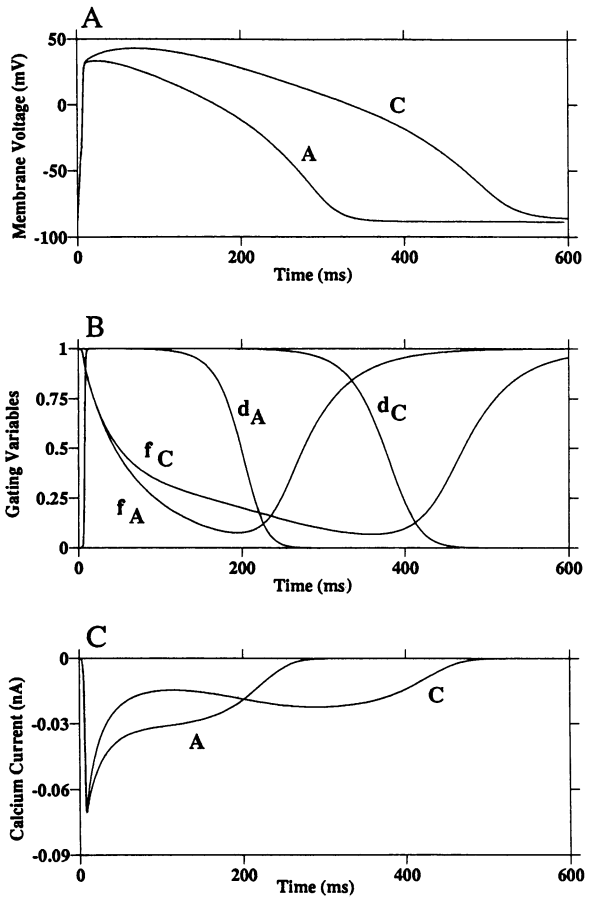

FIGURE 2 Model-generated action potential and gating variables controlling the calcium current under both control conditions (*C*) in a bathing medium containing ACh at a concentration of 0.1 μM. Panel *A* shows the model-generated atrial action potentials under bath conditions; the waveform labeled *C* is the control action potential, while that labeled *A* is the action potential in the presence of 0.1 μM ACh. Panel *B* illustrates the activation variable *d* and the inactivation variable *f* as functions of time. The subscripts *C* or *A* have the same connotation as in panel *A*. Panel *C* shows the I_{Ca} waveform under the same conditions.

decline in *f* establishes the initial peak in the I_{Ca} waveform ($d = 1$) and further decreases in *f* decrease the magnitude of I_{Ca}. A relative minimum in the magnitude of I_{Ca} is achieved at ~100 ms (Fig. 2 *C*). Note in addition that the "secondary hump" of the I_{Ca} waveform occurs during initial membrane repolarization. For a complete explanation of this "hump" it is important to recall that as membrane voltage hyperpolarizes, the ion transfer characteristic of the channel $\bar{I}_{Ca}$ gradually increases in magnitude. Thus, the increase in $\bar{I}_{Ca}$, even in the presence of a very slow decline in *f*, produces a net increase in the magnitude in I_{Ca}. Eventually, as the cell continues to repolarize, the activation variable *d* approaches 0 and closes the channels. Once again, the importance of the incomplete inactivation of *f* is emphasized. If in fact the

channel were to become completely inactivated during repolarization, the increase in $\bar{I}_{Ca}$ would have no effect on the calcium current.

An ACh-induced increase in the peak magnitude of I_{Ca} would appear to be contradictory to the well known reduction in the β agonist induced I_{Ca} by ACh (22). The explanation for this modeling result can be appreciated by examining the inactivation (f) and activation (d) variables controlling I_{Ca}. The important components of the I_{Ca} waveform at a bath ACh concentration of 0.1 μM ACh are shown in Fig. 2. Here, the increase in the gating variable d from 0 to 1 during the rapid upstroke produces the initial spike in the calcium current waveform and as d begins to deactivate, I_{Ca} begins to decrease in magnitude. This is identical to that shown in the control waveform shown in the same figure. However, in contrast to the control condition, the action potential shown in Fig. 2 *A* in the presence of ACh begins to repolarize earlier and as the cell is repolarized, the ion transfer characteristic ($\bar{I}_{Ca}$) of the calcium channel increases in magnitude. When the rate of repolarization by $I_{K,ACh}$ is fast, the rate of increase in $\bar{I}_{Ca}$ is more important than the slow decrease in the inactivation variable f. Consequently, I_{Ca} *increases* in magnitude. The I_{Ca} waveform shown in Fig. 2 *C* does not exhibit a prominent "secondary hump." Because the membrane voltage is repolarized at a faster rate in the presence of ACh, the activation variable, d, deactivates earlier under these conditions. In fact, d is deactivated before the combination of $\bar{I}_{Ca}$ and the incomplete inactivation of f can increase the magnitude of I_{Ca} and produce the secondary hump in I_{Ca} that is seen in control conditions.

The effect of different bath concentrations of ACh on the action potential is shown in Fig. 3 *A*. For this simulation, the stimulus rate was 0.5 Hz, which corresponds to the normal heart rate in the frog. The results indicate that the effect of activating the ACh-mediated K^+ current is to produce a graded reduction in the peak height and duration of the action potential. Note that ACh has very little effect on the rate of the rapid upstroke, illustrating that $I_{K,ACh}$ cannot compete with I_{Na}, which is a relatively large, fast current (3–4 nA) during the initial upstroke of the action potential.

Note in Fig. 3 that the control action waveform (*C*) exhibits a secondary depolarization lasting from ~20 to 90 ms after the initial upstroke. This is produced in the model by the slow inward calcium current I_{Ca}. The model-generated potential waveforms obtained at various ACh bath concentrations have a reduced (or even absent) period of secondary depolarization. Note also that in the presence of maximal [ACh], the resting membrane voltage is hyperpolarized 2 mV from the control resting level which is within the range reported by Giles and Noble on frog atrium (19).

The steady state $I_{K,ACh}$ (Eq. 5) is essentially constant

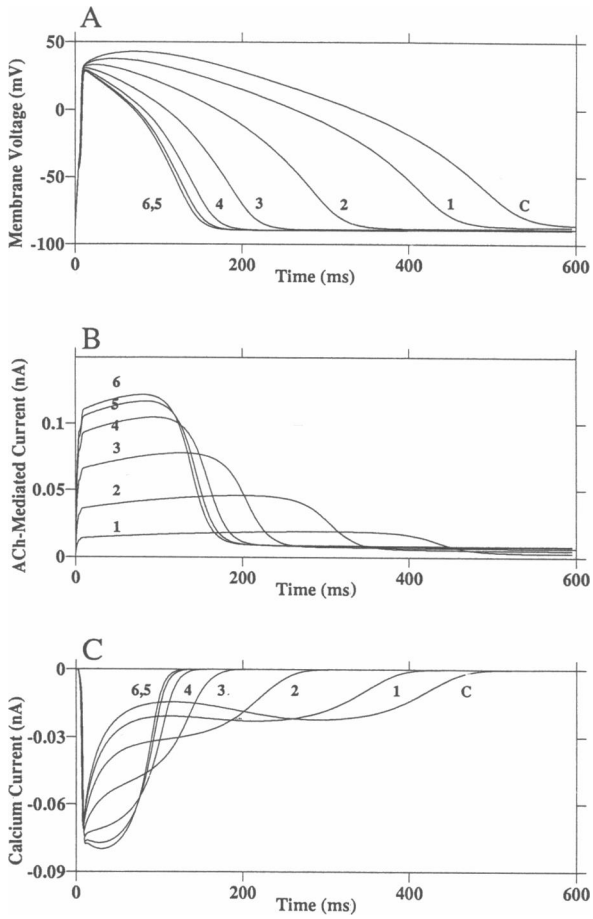

FIGURE 3 Model-generated simulations showing the effect of different assumed concentrations of ACh on the atrial action potential waveform as well as the membrane currents $I_{K,ACh}$ and I_{Ca}. The stimulus rate (0.5 Hz) used in the simulation corresponds to the normal heart rate in the bullfrog. *A* illustrates the model-generated steady-state atrial action potentials. *B* shows model-generated $I_{K,ACh}$ waveforms during an action potential. Note that during an action potential, this current activates very quickly and then enters a slowly increasing "plateau" phase before inactivation. *C* shows the model-generated indirect voltage–dependent effects of ACh concentration on the calcium current (I_{Ca}) during an action potential. Note that during an action potential in the presence of ACh, the I_{Ca} waveform is slightly increased in peak magnitude, but decreases significantly in duration. Notation is as follows: 1 = 0.03 μM, 2 = 0.1 μM, 3 = 0.3 μM, 4 = 1.0 μM, 5 = 3.0 μM, and 6 = 10.0 μM ACh.

(flat) for membrane voltage positive to −25 mV (data not shown), and the dynamics of $I_{K,ACh}$ are relatively fast. Because the transmembrane potential of the myocyte is more positive than −25 mV during most of the action potential, the $I_{K,ACh}$ waveform may be approximated as a "rounded square pulse" during the action potential as shown in Fig. 2 *B*. A complete family of simulated $I_{K,ACh}$ waveforms is shown in Fig. 3 *B*, which illustrates that over the ACh concentration range employed in the simulation, $I_{K,ACh}$ is almost fully activated within 20 ms.

Because $I_{K,ACh}$ is an outward current at the resting potential, the cell is slightly hyperpolarized in the presence of ACh compared with the control condition. Fig. 3 *B* also shows that the peak magnitude of $I_{K,ACh}$ increases as the bath ACh concentration increases; however, it is maximal above ~1 μM ACh concentration. The increase in magnitude is due to the ACh-dependence of the activation rate constant k_*. With increasing ACh concentration, the channel has a greater probability of opening, and thus $I_{K,ACh}$ increases. Note also that the resting level of outward current contributed by $I_{K,ACh}$ increases with the ACh concentrations.

The model-generated family of I_{Ca} waveforms which underlie the plateaus of the action potentials at different ACh bath concentrations are shown in Fig. 3 *C*. Two major effects are illustrated. First, the duration of the I_{Ca} waveforms (Fig. 3 *C*) becomes significantly shorter with an increasing ACh bath concentration, decreasing from ~500 to 150 ms. The explanation for this change is straightforward: the duration of the action potential decreases with increasing ACh concentration and therefore I_{Ca} deactivates earlier. The second indirect effect of ACh on the I_{Ca} waveform is somewhat surprising. As shown in Fig. 3 *C*, the peak magnitude *increases* as the ACh concentration is raised. Note also that with increasing [ACh] the duration of the I_{Ca} waveform decreases and the "secondary hump" in the I_{Ca} waveform is progressively attenuated. The "hump" disappears at an ACh concentration of 1 μM.

Although not shown, I_K is dramatically affected by the increased rate of repolarization of the cell. This is a direct result of the slow voltage-dependent time constant of the activation variable (n) of this current. Thus, as ACh concentration is increased, repolarization is brought about progressively earlier by the increasing muscarinic current $I_{K,ACh}$. Correspondingly, less I_K is activated.

The intracellular calcium concentration $[Ca]_i^{2+}$ during an action potential in the presence of specific bath ACh concentrations is shown in Fig. 4. Note that as [ACh] increases, $[Ca]_i^{2+}$ decreases. Integration of the I_{Ca} waveform (Fig. 3 *C*) with respect to time reveals that in the presence of maximal ACh concentration (10 μM), the change due to Ca^{2+} ions entering the cell was ~65% of the control condition. Assuming that the $[Ca]_i^{2+}$ transient is the input driving function of the contractile mechanism of the cell, the model predicts a decrease in contractile strength with increasing [ACh] in the bathing medium, i.e., a negative inotropic effect.

This model can also be used to examine the extent to which blockage of the sodium current affects the degree of action potential collapse in the presence of ACh. These results are shown in the "slow action potential" waveforms of Fig. 5 *A* which are obtained using a stronger stimulus pulse (1.75 nA compared with 1.2 nA) and of the

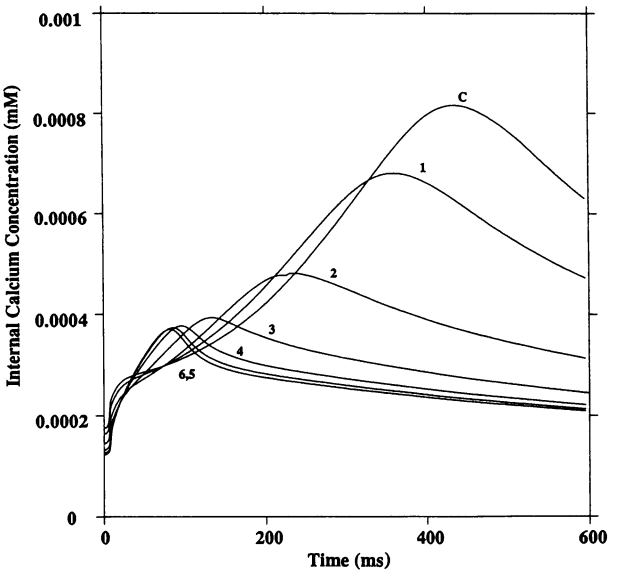

FIGURE 4 Model-generated internal $[Ca]_i^{2+}$ transients during an action potential in the presence of ACh. Note that $[Ca]_i^{2+}$ decreases as [ACh] increases. Notation same as in Fig. 3.

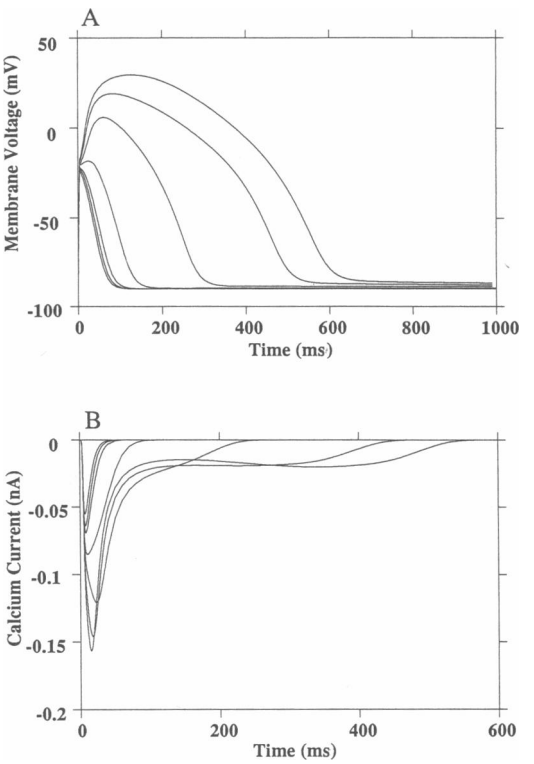

FIGURE 5 Model-generated "slow action potentials" and associated calcium current waveforms in the presence of Na channel blockage (e.g., with TTX). *A* shows the slow potentials that were elicited using a 1.75-nA current pulse with a duration of 4 ms. The family of action slow potentials are shown in various bath ACh concentrations. *B* illustrates the I_{Ca} waveforms during the action potentials. Note the I_{Ca} *decreases* in the presence of ACh.

same duration (4 ms). Under these conditions ACh has a more dramatic effect on the peak of the action potential waveform as can be seen by comparing this figure with Fig. 3 *A*, where the sodium channel is intact. Note that ACh has a graded effect on both the level of peak depolarization and the duration of the action potential. In addition, a hyperpolarized resting membrane level is shown with increasing concentrations of ACh. In Fig. 5 *A* there is a phase of secondary depolarization after the stimulus pulse for the simulations with the lower ACh bath concentrations (30, 100, and 300 nM). However, for an ACh concentration above 300 nM, no action potential was elicited and only the stimulus artifact remains.

The slow action potentials have (as their name implies) slower dynamics than normal action potentials and the currents elicited during the slow potential exhibit different waveforms than those seen during a normal action potential. The $I_{K,ACh}$ waveform (not shown), however, is essentially the same as that seen in the presence of I_{Na}. However, its magnitude is slightly reduced. On the other hand, as shown in Fig. 5 *B*, the magnitude and time course of the I_{Ca} waveform in the presence of TTX is completely different from that seen when I_{Na} is present (Fig. 3 *C*). Specifically, both the magnitude and duration of the I_{Ca} waveform *decrease* with increasing levels of ACh. During a slow action potential the stimulus depolarizes the myocyte to ~ -20 mV, whereas during a normal action potential the stimulus activates the sodium current I_{Na} which depolarizes the cell to ~25 mV. This decrease in initial transmembrane voltage for the slow potential (compared with the normal action potential) decreases the value of the activation variable *d*. With ACh in the bathing medium, the cell is repolarized faster (compared with 0 ACh) through the competitive interaction between $I_{K,ACh}$ and I_{Ca}, and the magnitude of the I_{Ca} waveform decreases.

DISCUSSION

In this study, a model of the ACh-sensitive K^+ current in a frog atrial myocyte has been developed and utilized to study some of the putative muscarinic ACh-induced effects on bullfrog atrial electrophysiological responses. Data for the characterization of the muscarinic K^+ current in amphibian heart came from recent literature (3, 4, 45). Compared with an earlier two-state model of the rabbit SA node by Osterrieder, Noma, and Trautwein (38), our model: (*a*) uses a nonlinear rather than linear ion transfer process to describe the muscarinic channel; and (*b*) employs an activation rate constant k_* leading to channel opening that is both voltage and ACh dependent rather than simply ACh dependent. Our simple model also differs from the higher-order kinetic model proposed by Pott and Pusch (39) in that our model uses two conductance states instead of four consecutive reactions, and the k_* rate coefficient is a function of both voltage and ACh concentration. The deactivation rate coefficient k_d leading to channel closing and the activation rate coefficient k_* leading to channel opening were modeled using data for bullfrog atrial myocyte from Simmons and Hartzell (45) and Breitwieser and Szabo (4). It is important to note that the original Osterrieder, Noma, and Trautwein model for the muscarinic K^+ current provided a qualitative fit to steady-state I–V curves of Breitwieser and Szabo (4), while Eq. 5 provided a better fit to the same data (results not shown) in that our model yielded an essentially constant steady state $I_{K,ACh}$ positive to -25 mV. Our modified model of the muscarinic K^+ current was incorporated into a larger model of the electrophysiological behavior of the bullfrog atrial myocyte (40), which in turn was subjected to a number of tests. These tests consisted of simulations of the electrical behavior of the atrial myocyte in bathing media containing different concentrations of ACh. The model predicts the observed shortening of the action potential of the cell with increasing levels of ACh (Fig. 3 *A*) and also provides insights into the probable mechanisms by which this shortening occurs (Figs. 2–5).

The model used in these studies assumes that ACh has a direct effect only on the muscarinic channel of the atrial cell membrane. However, it also demonstrates that the reduction in action potential duration produced by the muscarinic current $I_{K,ACh}$ on membrane potential has an indirect effect on the other channels (e.g., I_{Ca}) due to their voltage dependence. Hence, as the magnitude of $I_{K,ACh}$ increases progressively with increasing [ACh], it becomes sufficient to bring about repolarization at progressively earlier times (Fig. 2). Note from Fig. 2 *C*, however, that the initial spike portion of the I_{Ca} waveform remains only slightly affected, regardless of the magnitude of the $I_{K,ACh}$ current over the range of $0.03 \leq [ACh] \leq 10\ \mu M$.

The model results indicate that in the absence of β agonists, the effect of ACh on membrane voltage (action potential collapse) can be qualitatively explained by the direct action of ACh-sensitive potassium current $I_{K,ACh}$ that produces a fast dynamic repolarization current. This result is consistent with recent experiments on frog atrium and ventricle myocytes (22), guinea pig atrial myocytes (26), and ferret ventricular myocytes (2). Additionally, $I_{K,ACh}$ interacts indirectly with the calcium channel via its voltage dependence to slightly increase the peak magnitude of the I_{Ca} waveform. Although an increased inward current would tend to increase the duration of the action potential, the magnitude and time course of the muscarinic-induced current is sufficient to initiate repolarization. When the sodium channels are not blocked with TTX there is a significant interaction between I_{Ca} and

$I_{K,ACh}$ as shown in Fig. 3, where there is a decrease in peak action potential depolarization. When the sodium channels are blocked by TTX, there is an even greater interaction between I_{Ca} and $I_{K,ACh}$ as shown by the graded peak depolarization of the action potential as a function of ACh concentration (Fig. 5). Additionally, the form of the I_{Ca} waveform during an action potential is dependent on the dynamics of the action potential. In the presence of ACh, I_{Ca} increases when the sodium channels are active and decreases when the sodium channels are blocked.

The model also predicts a *decreasing* intracellular calcium ion concentration in the presence of a calcium current I_{Ca} that has an increasing peak magnitude (Fig. 4). In our simulations this occurs because the amount of Ca^{2+} entering the cell is reduced due to the earlier repolarization resulting from $I_{K,ACh}$. Because the contractile response follows changes in $[Ca^{2+}]_i$, contractile strength would be expected to decrease with increasing ACh concentration. Thus, the model predicts a negative inotropic effect with increasing [ACh]. This explanation for the negative inotropic effect of ACh on ferret ventricular myocytes has recently been proposed by Boyett et al. (2).

As indicated previously in the Introduction, the current study is concerned only with the direct effects of acetylcholine on the muscarinic channel in the bullfrog atrial myocyte. Thus, the effects of ACh on I_{Ca} in the presence of a β agonist have not been modeled and may contribute significantly to the overall response of the atrial cell to administration of ACh. In addition, our study neglects the effects of ACh on the Na^+/K^+ pump (23) and the hyperpolarization-activated current I_f (12, 13, 14). A full characterization of the muscarinic effects of ACh on the amphibian or mammalian heart should address these effects. In the present study, only the direct effect of ACh on the muscarinic channel is modeled to discern the effect that this pathway would have on the overall electrophysiological behavior of the atrial cell. We express this caution because it may turn out in a more complete study that the direct effect of ACh on the muscarinic channel may be of lesser importance, because in vivo the level of intracellular calcium concentration is set by sympathetic tone, making the indirect second-messenger mediated pathway for ACh effects more prominent.

This work was supported by the National Science Foundation under grants BNS8716568 and ECS8405435 awarded to Dr. Clark. Dr. Giles is supported as a Medical Scientist by the Alberta Heritage Foundation and receives ongoing support from the Canadian Medical Research Council and the Canadian Heart Foundation.

Received for publication 19 June 1989 and in final form 7 November 1989.

REFERENCES

1. Birnbaumer, L., J. Codina, R. Mattera, A. Cerione, J. D. Hildebrandt, T. Sunyer, F. J. Rojas, M. G. Caron, R. J. Lefkowitz, and R. Iyengar. 1985. Molecular Mechanisms of Transmembrane Signalling. P. Cohen and M. D. Houslay, editors. Elsevier Scientific Publishing Co., New York. 131–182.
2. Boyett, M. R., M. S. Kirby, C. H. Orchard, and A. Roberts. 1988. The negative inotropic effect of acetylcholine on ferret ventricular myocardium. *J. Physiol. (Lond.).* 404:613–635.
3. Breitwieser, G. E., and G. Szabo. 1985. Uncoupling of cardiac muscarinic and β-adrenergic receptors from ion channels by a guanine nucleotide analogue. *Nature (Lond.).* 317:538–540.
4. Breitwieser, G. E., and G. Szabo. 1988. Mechanism of muscarinic receptor-induced K^+ channel activation as revealed by hydrolysis-resistant GTP analogues. *J. Gen. Physiol.* 91:469–493.
5. Brown, A. M., and L. Birnbaumer. 1988. Direct G protein gating of ion channels. *Am. J. Physiol.* 254:H401–H410.
6. Campbell, D. L., W. R. Giles, J. R. Hume, and E. F. Shibata. 1988. Inactivation of calcium current in bull-frog atrial myocytes. *J. Physiol. (Lond.).* 405:287–315.
7. Carmeliet, E., and K. Mubagwa. 1986. Changes by acetylcholine of membrane currents in rabbit cardiac Purkinje fibers. *J. Physiol. (Lond.).* 371:201–217.
8. Carmeliet, E., and K. Mubagwa. 1986. Desensitization of the acetylcholine-induced increase of potassium conductance in rabbit cardiac Purkinje fibers. *J. Physiol. (Lond.).* 371:239–255.
9. Champigny, G., R. Bois, and J. Lenfant. 1987. Characterization of the ionic mechanism responsible for the hyperpolarization-activated current in frog sinus venosus. *Pfluegers Arch. Eur. J. Physiol.* 410:159–164.
10. Champigny, G., and J. Lenfant. 1986. Block and activation of the hyperpolarization-activated inward current by Ba^{2+} and Cs in frog sinus venosus. *Pfluegers Arch. Eur. J. Physiol.* 407:684–690.
11. Codina, J., A. Yatani, D. Grenet, A. M. Brown, and L. Birnbaumer. 1987. The α subunit of the GTP binding protein G_k opens atrial potassium channels. *Science (Wash. DC).* 236:442–444.
12. DiFrancesco, D., R. Ducouret, and R. B. Robinson. 1989. Muscarinic modulation of cardiac rate at low acetylcholine concentrations. *Science (Wash. DC).* 243:669–671.
13. DiFrancesco, D., and C. Tromba. 1987. Acetylcholine inhibits activation of the cardiac hyperpolarizing-activated current, I_f. *Pfluegers Arch. Eur. J. Physiol.* 410:139–152.
14. DiFrancesco, D., and C. Tromba. 1988. Inhibition of the hyperpolarization-activated current (I_f) induced by acetylcholine in rabbit sino-atrial node myocytes. *J. Physiol. (Lond.).* 405:477–491.
15. DiFrancesco, D., and C. Tromba. 1988. Muscarinic control of the hyperpolarization-activated current (I_f) in rabbit sino-atrial node myocytes. *J. Physiol. (Lond.).* 405:493–510.
16. Dunlap, K., G. G. Holz, and S. G. Rane. 1987. G proteins as regulators of ion channel function. *Trends Neurosci.* 10:241–244.
17. Ferguson, K. M., T. Higashijima, M. D. Smigel, and A. G. Gilman. 1986. The influence of bound GDP on the kinetics of guanine nucleotide binding to G proteins. *J. Biol. Chem.* 261:7393–7399.
18. Fischmeister, R., and H. C. Hartzell. 1986. Mechanism of action of acetylcholine on calcium current in single cells from frog ventricle. *J. Physiol. (Lond.).* 376:183–202.
19. Giles, W., and S. Noble. 1976. Changes in membrane currents in

bullfrog atrium produced by acetylcholine. *J. Physiol. (Lond.).* 261:103–123.

20. Giles, W. R., and E. F. Shibata. 1985. Voltage clamp of bull-frog cardiac pace-maker cells: a quantitative analysis of potassium currents. *J. Physiol. (Lond.).* 368:265–292.
21. Gilman, A. G. 1987. G proteins: transducers of receptor-generated signals. *Annu. Rev. Biochem.* 56:615–649.
22. Hartzell, H. C., and M. A. Simmons. 1987. Comparison of effects of acetylcholine on calcium and potassium currents in frog atrium and ventricle. *J. Physiol. (Lond.).* 389:411–422.
23. Hasuo, H., K. Koketsu, and S. Minota. 1988. Indirect effects of acetylcholine on the electrogenic sodium pump in bull-frog atrial muscle fibres. *J. Physiol. (Lond.).* 399:519–535.
24. Hescheler, J., M. Kameyama, and W. Trautwein. 1986. On the mechanism of muscarinic inhibition of the cardiac Ca current. *Pfluegers Arch. Eur. J. Physiol.* 407:182–189.
25. Hino, N., and R. Ochi. 1980. Effect of acetylcholine on membrane currents in guinea-pig papillary muscle. *J. Physiol. (Lond.).* 307:183–197.
26. Iijima, T., H. Irisawa, and M. Kameyama. 1985. Membrane currents and their modification by acetylcholine in isolated single atrial cells of guinea-pig. *J. Physiol. (Lond.).* 359:485–501.
27. Kameyama, M., F. Hofmann, and W. Trautwein. 1985. On the mechanism of β-adrenergic regulation of the Ca channel in the guinea-pig heart. *Pfluegers Arch. Eur. J. Physiol.* 405:285–293.
28. Kim, D., D. L. Lewis, L. Graziadei, E. J. Neer, D. Mar-Sagi, and D. E. Clapham. 1989. G-protein $\beta\gamma$-subunits activate the cardiac muscarinic K^+-channel via phospholipase A_2. *Nature (Lond.).* 337:557–560.
29. Kirsch, G. E., A. Yatani, J. Codina, L. Birnbaumer, and A. M. Brown. 1988. α-Subunit of G_k activates atrial K^+ channels of chick, rat, and guinea pig. *Am. J. Physiol.* 254:H1200–H1205.
30. Kurachi, Y., H. Ito, T. Sugimoto, T. Katada, and M. Ui. 1989. Activation of atrial muscarinic K^+ channels by low concentrations of $\beta\gamma$ subunits of rat brain G protein. *Pfluegers Arch. Eur. J. Physiol.* 413:325–327.
31. Kurachi, Y., T. Nakajuma, and T. Sugimoto. 1986. Role of intracellular Mg^{2+} in the activation of muscarinic K^+ channel in cardiac atrial cell membrane. *Pfluegers Arch. Eur. J. Physiol.* 407:572–574.
32. Lapidus, L., and J. Senfeld. 1971. Numerical Solution of Ordinary Differential Equations. Academic Press, Inc., New York.
33. Logothetis, D. E., D. Kim, J. K. Northup, E. J. Neer, and D. E. Clapham. 1988. Specificity of action of guanine nucleotide-binding regulatory protein subunits on the cardiac muscarinic K^+ channel. *Proc. Natl. Acad. Sci. USA.* 85:5814–5818.
34. Logothetis, D. E., Y. Kurachi, J. Galper, E. J. Neer, and D. E. Clapham. 1987. The $\beta\gamma$ subunits of GTP-binding proteins activate the muscarinic K^+ channel in heart. *Nature (Lond.).* 325:321–326.
35. Momose, Y., W. Giles, and G. Szabo. 1984. Acetylcholine-induced K^+ current in amphibian atrial cells. *Biophys. J.* 45:20–22.
36. Nargeot, J., H. A. Lester, H. J. M. Birdsall, J. Stockton, N. H. Wasserman, and B. F. Erlanger. 1982. A photoisomerizable muscarinic atagonist. Studies of binding and of conductance relaxations in frog heart. *J. Gen. Physiol.* 79:657–678.
37. Ochi, R. 1981. The Mechanism of Gated Calcium Transport across Biological Membranes. Academic Press, New York.
38. Osterrieder, W., A. Noma, and W. Trautwein. 1980. On the kinetics of the potassium channel activated by acetylcholine in the S-A node of the rabbit heart. *Pfluegers Arch. Eur. J. Physiol.* 386:101–109.
39. Pott, I., and H. Pusch. 1979. A kinetic model for the muscarinic action of acetylcholine. *Pfluegers Arch. Eur. J. Physiol.* 383:75–77.
40. Rasmusson, R., J. W. Clark, W. R. Giles, K. Robinson, D. L. Campbell, R. B. Clark, and E. F. Shibata. 1990. A mathematical model of electrophysiological activity in a bullfrog atrial cell. *Am. J. Physiol.* In press.
41. Reuter, H. 1983. Calcium channel modulation by neurotransmitters, enzymes and drugs. *Nature (Lond.).* 301:569–574.
42. Rush, S., and H. Larsen. 1978. A practical algorithm for solving dynamic membrane equations. *IEEE (Inst. Electr. Electron. Eng.) Trans. Biomed. Eng.* 25:389–393.
43. Sakmann, B., A. Noma, and W. Trautwein. 1983. Acetylcholine activation of single muscarinic K^+ channels in isolated pacemaker cells of the mammalian heart. *Nature (Lond.).* 303:250–253.
44. Shibata, E. F., and W. R. Giles. 1985. Ionic currents that generate the spontaneous diastolic depolarization in individual cardiac pacemaker cells. *Proc. Natl. Acad. Sci. USA.* 82:7796–7800.
45. Simmons, M. A., and H. C. Hartzell. 1987. A quantitative analysis of the acetylcholine-activated potassium current in single cells from frog atrium. *Pfluegers Arch. Eur. J. Physiol.* 409:454–461.
46. Ten Eick, R., H. Nawrath, T. F. McDonald, and W. Trautwein. 1976. On the mechanism of the negative inotropic effect of acetylcholine. *Pfluegers Arch. Eur. J. Physiol.* 361:207–213.
47. Trautwein, W., and M. Kameyama. 1986. Intracellular control of calcium and potassium currents in cardiac cells. *Jpn. Heart J.* 27(Suppl.):31–50.
48. Yatani, A., J. Codina, Y. Imoto, J. P. Reeves, L. Birnbaumer, and A. M. Brown. 1987. A G protein directly regulates mammalian cardiac calcium channels. *Science (Wash. DC).* 238:1288–1292.